

# Biochar increased water holding capacity but accelerated organic carbon leaching from a sloping farmland soil in China

Chen Liu<sup>1</sup> · Honglan Wang<sup>1</sup> · Xiangyu Tang<sup>1</sup> · Zhuo Guan<sup>1</sup> · Brian J. Reid<sup>2</sup> · Anushka Upamali Rajapaksha<sup>3</sup> · Yong Sik Ok<sup>3</sup> · Hui Sun<sup>4</sup>

Received: 21 December 2014 / Accepted: 15 June 2015 / Published online: 25 June 2015  
© Springer-Verlag Berlin Heidelberg 2015

**Abstract** A hydrologically contained field study, to assess biochar (produced from mixed crop straws) influence upon soil hydraulic properties and dissolved organic carbon (DOC) leaching, was conducted on a loamy soil (entisol). The soil, noted for its low plant-available water and low soil organic matter, is the most important arable soil type in the upper reaches of the Yangtze River catchment, China. Pore size distribution characterization (by N<sub>2</sub> adsorption, mercury intrusion, and water retention) showed that the biochar had a tri-modal pore size distribution. This included pores with diameters in the range of 0.1–10 μm that can retain plant-available water. Comparison of soil water retention curves between the control (0) and the biochar plots (16 t ha<sup>-1</sup> on dry weight basis) demonstrated biochar amendment to

increase soil water holding capacity. However, significant increases in DOC concentration of soil pore water in both the plough layer and the undisturbed subsoil layer were observed in the biochar-amended plots. An increased loss of DOC relative to the control was observed upon rainfall events. Measurements of excitation-emission matrix (EEM) fluorescence indicated the DOC increment originated primarily from the organic carbon pool in the soil that became more soluble following biochar incorporation.

**Keywords** Biochar · Soil · Pore size distribution · Water holding capacity · DOC · EEM fluorescence

## Introduction

Biochar, a carbon-rich porous material produced from the pyrolysis of biomass, has gained considerable interest in recent years as a chemically and biologically stable carbon pool (Lehmann et al. 2006) and also a soil amendment for various purposes, including improvement of soil quality, increase of crop yield, and remediation of contaminated soil (Laird et al. 2010; Ahmad et al. 2014; Veksha et al. 2014; Nelissen et al. 2015). Despite the growing number of studies on soil amendment with biochar, biochar's effect is soil type dependent, and the claimed positive effects are still largely unknown for many infertile and drought-prone soils (e.g., entisols). More importantly, there is a clear need to upscale results from laboratory and pot studies to long-term field experiments.

In general, few scientific literatures have been published with respect to the influences of biochar on soil physical properties under field circumstances in temperate regions (Atkinson et al. 2010; Asai et al. 2009). The meta-analysis by Jeffery et al. (2011) indicated biochar to be able to improve acidic soils by a liming effect and soils with a coarse or

---

Responsible editor: Zhihong Xu

**Electronic supplementary material** The online version of this article (doi:10.1007/s11356-015-4885-9) contains supplementary material, which is available to authorized users.

- ✉ Xiangyu Tang  
xytang@imde.ac.cn
- ✉ Hui Sun  
sunhuifiles@gmail.com

- <sup>1</sup> Key Laboratory of Mountain Surface Processes and Ecological Regulation, Institute of Mountain Hazards and Environment, Chinese Academy of Sciences, Chengdu, China
- <sup>2</sup> School of Environmental Science, University of East Anglia, Norwich, England, UK
- <sup>3</sup> Korea Biochar Research Center and Department of Biological Environment, Kangwon National University, Chuncheon, Republic of Korea
- <sup>4</sup> College of Architecture and Environment, Sichuan University, Chengdu, China

medium texture by increasing soil water holding capacity. However, several other studies from field trial have showed little effects of biochar on soil hydraulic properties (Karhu et al. 2011; Case et al. 2013; Tammeorg et al. 2014). The inconsistency in the results among the studies is mainly attributed to the great differences in soil types and regional climate conditions. Biochar's properties that are determined by feedstock type and pyrolysis conditions also play important roles in their impacts on soil. Moreover, land and pot trials are often short-time, it is obviously important to better understand biochar's long-term effects under field cropping conditions so that reliable evaluation of benefits or negative effects of biochar amendment can be appreciated.

Soil porosity and pore size distribution (PSD) are physical characteristics that are crucial to the understanding of biochar's effects on soil properties. The pore distribution is even more important than the total porosity since water and gas transport in soil are controlled by the specific volume of pores within certain size range. Thus, characterization of PSD both for the biochar alone and the biochar-amended soil can help us better explain mechanisms for the potential effects of biochar on soil.

On the other hand, as compared to the large number of current studies focused on biochar's effects on carbon sequestration in soil, there have been relatively fewer investigations on its effects on the leaching of dissolved organic carbon (DOC) and underlying mechanism (Hockaday et al. 2007; Mukherjee and Zimmerman 2013), while this is a very important aspect concerning the long-term effects on the quality of both soil and the ambient aquatic environment. Changes in DOC compositions caused by biochar application, if they occur, could be important particularly if this DOC can be transported to drinking water sources. Where these waters are treated, aromatic carbon in DOC can be a problem as it is a major reactive source in the formation of disinfection byproducts (DBPs), which reduce water quality and are toxic to human health (Korshin et al. 2002). Biochar-derived aromatic carbon has been detected in ground water and rivers through leaching from soil (Hockaday et al. 2007; Guggenberger et al. 2008). Chow et al. (2006) reported not only DOC production but the proportion of DBP precursor to be increased under flooding conditions and wet-dry cycles. Therefore, there is a need to examine biochar's potential effects on the DOC formation and leaching from the amended soils (particularly in the field). Excitation-emission matrix (EEM) fluorescence spectroscopy has been extensively used to track and characterize DOC in both natural and engineered water systems (Henderson et al. 2009) but seldom used in researches with related subjects to this study.

To address the gaps in knowledge, a Chinese commercial biochar produced from pyrolysis of mixed crop straws was applied to a sloping farmland entisol at field-plot scale. This study was carried out after 1 year of biochar application. The

objectives include (1) to characterize biochar properties and particularly its PSD feature by using a combination of three complementary PSD characterization methods; (2) to examine the effects of biochar amendment on soil water holding capacity; (3) to examine the biochar effects on DOC transport out of the soil plots; and (4) to appportion changes in DOC concentration to either biochar itself or natural soil organic matter sources using EEM fluorescence spectroscopy.

## Materials and methods

### Source of biochar

The commercial biochar used in this study (referred to as BC hereafter) was purchased from Sanli New Energy Company located at Shangqiu, Henan, China. Biochar was made from slow pyrolysis (at 500 °C) in fluidized bed furnace on a scale of 1000 t day<sup>-1</sup>. From every ton of mixed crop straws as feedstock, 0.3 t biochar was produced, along with co-products including 0.25 t pyroligneous acid, 0.03 t wood tar and 780 m<sup>3</sup> gases.

### Characterization of biochar properties

Proximate analysis of the biochar was conducted in duplicate following American Society for Testing and Materials (ASTM) method D5142. Moisture was measured by heating the biochar at 105 °C to a constant weight. The dehydrated BC (kept in covered crucibles) was then heated in a furnace at 450 °C for 1 h to determine its mobile matter based on weight loss. Ash content was then measured after heating the BC in uncovered crucibles at 750 °C for 1 h. Finally, resident matter was calculated by the difference between the initial weight and the summed weight of moisture, mobile matter and ash contents.

Ultimate analysis (C, H, N, S, and O) was determined on the dry basis of BC by an elemental analyzer (Flash EA 1112 series, CE Instruments, UK). Oxygen was determined by weight difference. pH and electric conductivity were measured in a suspension of BC/deionized water (1 g:5 mL) using a digital pH/conductivity meter (Orion, Thermo Electron Corp., Waltham, MA, USA). Particle size distribution was determined by a ParticalA-950A laser scattering particle size analyzer (Horiba Instruments, Kyoto, Japan). Surface morphology was examined by a scanning electron microscope (SEM; S-2350, Hitachi, Tokyo, Japan) after gold coating.

The biochar textural properties were measured by N<sub>2</sub> adsorption/desorption isotherms at 77 K using a nanoporosity system (NOVA-1200, Quantachrome Corp., Boynton Beach, FL, USA). The BC was vacuum-degassed for 6 h at 473 K prior to measurement. The obtained isotherm data were fitted to Brunauer-Emmett-Teller (BET) model for

the calculation of specific surface area and total pore volume, and Barret-Joyner-Halender (BJH) model for pore size distribution (PSD), respectively.

PSD was also measured using an AutoPore III mercury porosimeter (Micromeritics Instrument, Norcross, GA, USA). The biochar was oven-dried at 105 °C, vacuum-degassed, and intruded with mercury in step-wise pressure increments in the range from 0.0036 to 413 MPa. PSD was determined using the Washburn equation (1921):

$$P = \frac{2\gamma_{\text{Hg}}\cos\theta}{r} \quad (1)$$

where  $P$  is the external pressure (Pa) in the vacuum chamber,  $\gamma_{\text{Hg}}$  is the surface tension of mercury  $0.48 \text{ J m}^{-2}$ ,  $\theta$  is the contact angle of mercury ( $140^\circ$ ), and  $r$  is the radius (m) of cylindrical pore aperture.

Thirdly, the biochar was packed into cutting rings, saturated with tap water, and then analyzed for PSD by measuring the drying water retention curve under stepwise increased suction in a sandbox and pressure chambers (this is a standard method commonly used to characterize pore system of soil). Method details are described in the section that follows.

## Field plot scale experiment

### Experimental site

The experimental site is located within an agricultural catchment ( $31^\circ 16' \text{ N}$ ,  $105^\circ 27' \text{ E}$ ) in the hilly area of central Sichuan, southwest China. The area is dominated by a loamy soil that is classified as entisol (USDA Taxonomy). The soil was formed by fast weathering of the parent mudrock and is the most important arable land resource in the upper reaches of Yangtze River, China. According to meteo-records of the past two decades, annual mean temperature and precipitation at the site are  $17.3 \text{ }^\circ\text{C}$  and  $826 \text{ mm}$ , respectively, with ca. 85 % of annual rainfall occurring between May and September.

### Field biochar application to soil

Six experimental filed plots were randomly selected from a total of 36 long-term (over 10 years) sloping farmland plots in this study (as shown in the Supplementary Material, SM1). The field trial involved one factor with two treatments (with three replicates): 0 and  $16 \text{ t ha}^{-1}$  biochar application (on oven-dry weight base). The size of each plot was  $3 \times 8 \text{ m}^2$ . The biochar application rate of  $16 \text{ t ha}^{-1}$  corresponds to  $6.0 \text{ g kg}^{-1}$  soil ( $5.0 \text{ g C kg}^{-1}$  soil) assuming an incorporation depth of 0.2 m with a bulk density of  $1.35 \text{ g cm}^{-3}$ . During biochar application, each plot was subdivided into sub-plots of  $1 \text{ m}^2$  to which  $2.0 \text{ kg}$  of fresh biochar (equivalent to  $1.6 \text{ kg}$  dry mass) was weighed and applied by hand. This work was done

on a light rainy day in May 2013 so that biochar dust losses were avoided. The biochar was incorporated into soil through tillage several days after application. Cropping in rotations of winter wheat and summer maize were continued in these field plots as before. Biochar effects on soil properties were examined after the biochar had been aged in the soil over a year, so that likely transient effects within short term after biochar application could be avoided.

### Sampling of soil, soil water, and leachate

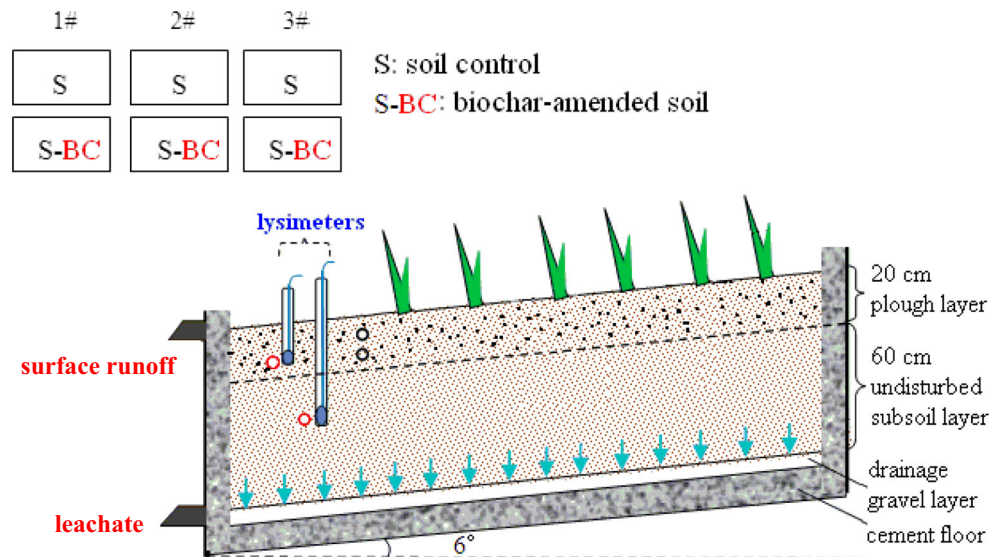
Three kinds of samples were taken from the field plots including (i) soil for the measurement of water-extractable organic carbon (WEOC); (ii) undisturbed soil core for the analysis of water retention curve; and (iii) soil pore water and leachate collected during rain events for the examination of DOC transport.

As shown in Fig. 1, soil samples (5 g each, three replicates) were taken from each plot at depths of 10 and 40 cm, representing the plough layer and undisturbed subsoil layer, respectively. WEOC was obtained from extracting 5 g soil in a 25 mL of  $5 \text{ mmol L}^{-1}$   $\text{CaCl}_2$  solution. The vessels were shaken for 2 h in a  $25 \text{ }^\circ\text{C}$  water bath and then centrifuged. The supernatants were  $0.45 \text{ }\mu\text{m}$  filtered and tested for DOC concentrations using an Auto Analyzer 3 TOC analyzer (SEAL Analytical, Norderstedt, Germany).

Soil core samples of  $100 \text{ cm}^3$  volume (three replicates) were taken from two depths (2.5–7.5 and 12.5–17.5 cm) in the plough layer of the three control plots and three biochar-amended plots. No samples were taken from the subsoil layer as we assumed that biochar application caused no marked physical changes in pore system of this soil layer. The collected cores were stored at  $4 \text{ }^\circ\text{C}$  in laboratory fridge before the measurement of water retention curve.

A total of 12 1900 series porous-cup lysimeters (SoilMoisture Equipment Corp., Goleta, CA, USA) were installed at the lower slope of each plot at depths of 10 and 40 cm (Fig. 1) to collect soil pore water. All the samplers were emptied with a syringe and vacuumed to keep a low-tension state (with a maximum tension of 80 kPa) prior to rainfall event. Soil solutions were collected as soon as the rain stopped. Leachate from the farmland, if generated, was also collected with a bucket. Samples were immediately  $0.45 \text{ }\mu\text{m}$  filtered and determined for DOC concentration. DOC flux from each plot was then calculated based on the DOC concentration and total volume of leachate discharge. The sampling campaigns were carried out for a series of rainfall events during the period from August to October 2014. Data of rainfall and average daily temperature were presented in Fig. 2, with dates marked on which samples of soil pore water and leachate were collected.

**Fig. 1** Schematic of six experimental plots (three replicates with two treatments), an individual biochar-amended plot (S-BC) and sampling for soil (red circles), undisturbed soil core (black circles), soil pore water (from lysimeters) and leachate (from collecting tank)



**Analysis of water retention curve**

Same methodology for the measurement of soil water retention curves (SWRCs) and analysis were carried out for undisturbed soil cores taken from the field plots and the packed cores of biochar alone. The ring size for the biochar was custom-made as 2.5 cm (height) × 1.2 cm (i.d.), 5 mm thickness. All the cores were saturated with tap water prior to measurement.

SWRCs were constructed by measuring soil water content at 12 soil matric heads (−1, −2.5, −10, −30, −60, −100, −340, −510, −1020, −2040, −5100, and −15,300 cm) according to Cornelis et al. (2005). A sand box apparatus (i.e., hanging-water column method) was used for the pressure heads ranging from −1 to −100 cm, while pressure plates (Soilmoisture Equipment Corp., Santa Barbara, CA, USA) were used for −340 to −15,300 cm. After equilibrium was reached at −15,300 cm in the end, soil cores were oven-dried at 105 °C for

24 h, after which bulk density and water content could be calculated on a volumetric basis.

Porosity ( $\emptyset$ ) was calculated as

$$\emptyset = 1 - \frac{\rho_b}{\rho_s} \tag{2}$$

where  $\rho_b$  and  $\rho_s$  are the bulk and particle densities ( $\text{g cm}^{-3}$ ), respectively.

The water content vs pressure head data were fitted using the function of van Genuchten (1980):

$$\theta(h) = \theta_r + \frac{\theta_s - \theta_r}{[1 + (\alpha h)^n]^m} \tag{3}$$

where  $\theta$  is the volumetric water content ( $\text{m}^3 \text{m}^{-3}$ ),  $h$  is pressure head (cm) (taken as a positive value),  $\theta_r$  and  $\theta_s$  are the residual and saturated water contents ( $\text{m}^3 \text{m}^{-3}$ ), respectively,  $\alpha$  ( $\text{cm}^{-1}$ ),  $n$ , and  $m$  ( $=1 - 1/n$ ) are empirical parameters.

Soil physical parameters were derived from the SWRCs, including soil matrix porosity ( $\theta_m$ ), macroporosity (MacPor), air capacity (AC) and plant-available water capacity (PAWC).  $\theta_m$  is defined as the volumetric water content retained by soil textural pores (exclusive of macropores), which corresponds to pore diameters of  $\leq 75 \mu\text{m}$ . Thus, MacPor refers to pores with diameter  $\geq 75 \mu\text{m}$ . AC is an indicator of soil aeration, and PAWC is a parameter indicating the capacity of the soil to store and provide available water to plant roots. These parameters were calculated as follows (Reynolds et al 2007):

$$\text{MacPor} = \theta_s - \theta_m \tag{4}$$

$$\text{AC} = \theta_s - \theta_{\text{FC}} \tag{5}$$

$$\text{PAWC} = \theta_{\text{FC}} - \theta_{\text{PWP}} \tag{6}$$

where  $\theta_m$  was determined at the matric head of −40 cm in this study;  $\theta_{\text{FC}}$  and  $\theta_{\text{PWP}}$  are the volumetric water contents at field

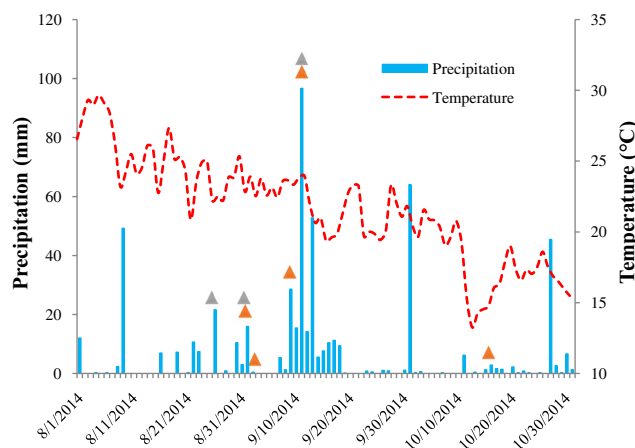


**Fig. 2** Precipitation and average daily temperature in the area of the experimental field from August to October 2014. Dates for sampling of soil pore water (orange triangle) and leachate (gray triangle) were marked

capacity ( $h=-340$  cm) and at permanent wilting point (PWP) ( $h=-15,300$  cm), respectively.

Moreover, since each SWRC has a unique inflection point where the shape of SWRC changes from convex to concave, another parameter was defined as the inflection slope ( $S_{inf}$ ), which can be used as a measure of soil microstructure. A more negative  $S_{inf}$  indicates a better soil physical quality. It was calculated using the following equation (Dexter 2004):

$$S_{inf} = -n(\theta_s - \theta_r) \left( \frac{2n-1}{n-1} \right)^{\left( \frac{1}{n} - 2 \right)} \quad (7)$$

PSDs were calculated as the derivative of the equivalent  $\theta(r)$  curve converted from the fitted SWRCs, where  $r$  ( $\mu\text{m}$ ) is the maximum equivalent radius of pore that remains full of water at a given pressure head  $h$  (cm). Here,  $r$  can be calculated from  $h$  using the Young-Laplace equation (Vomocil and Flocker 1965):

$$r = \frac{1490}{|h|} \quad (8)$$

### Analysis of fluorescence spectroscopy

For soil pore water and leachate samples, EEM fluorescence was measured using an Aqualog spectrofluorometer made by Horiba JY (Edison, NJ, USA) with a 3.5-mL quartz cuvette (light path 10 mm  $\times$  10 mm, bandpass 5 nm, integration time 0.5 s). The excitation and emission wavelength ranges were 200–460 and 270–600 nm, respectively, both at 5 nm increments. EEM spectra were obtained by presenting fluorescence intensity as a function of excitation-emission wavelength coordinates. Blank EEM spectrum obtained for MilliQ water was subtracted from each sample’s EEM to remove background fluorescence. UV absorbance was measured simultaneously for each sample and used to account for inner filter effects (IFE) using the Origin-based Aqualog<sup>®</sup> software package. Also, both Rayleigh-scattering lines were removed. Given that we only examined the relative changes of fluorescence, spectral data were not normalized to water Raman or quinine sulfate units.

The obtained EEM spectra were processed using the fluorescence regional integration (FRI) technique (Chen et al. 2003; Gerrity et al. 2012). Briefly, cumulative fluorescence intensity ( $\phi_i$ ) that quantifies overall response of particular fraction of fluorophores beneath EEM region  $i$  can be determined as (Hernandez-Ruiz et al. 2012):

$$\phi_i = \sum_{ex} \sum_{em} I(\lambda_{ex}\lambda_{em}) \Delta\lambda_{ex} \Delta\lambda_{em} \quad (9)$$

where  $\Delta\lambda_{ex}$  and  $\Delta\lambda_{em}$  are the excitation and emission wavelength intervals on the EEM contour map, respectively, and

$I(\lambda_{ex}\lambda_{em})$  is the fluorescence intensity at any selected excitation-emission wavelength coordinates.

### Statistical analysis

Independent and paired  $t$  tests were used to examine whether the biochar treatment was different from the control regarding soil hydro-physical properties and DOC leaching. The analysis was conducted using SPSS 17.0 for Windows (IBM Corp., Armonk, NY, USA), with all significance being two-tailed.

## Results and discussion

### Basic properties of biochar

Most of the measured parameters (as listed in Table 1) of the commercial biochar used in this study are in the same range as those reported for other biochar products made from pyrolysis of crop straws (e.g., wheat, rice, maize) at around 500 °C in the literature (Ahmad et al. 2014), indicating the pyrolysis temperature and feedstock type may have determining effects on the properties of final product. For instance, the biochar has a pH in the alkaline range, and a high ash content (being attributable to abundant mineral salts of Si, K, Ca, and Al in the biomass of crop straws (Lee et al. 2013)). The C content of around 83 % as well as low molar ratios of H/C and O/C indicates the biochar’s carbonaceous and aromatic texture.

**Table 1** Characteristics of the commercial biochar used in this study

	BC
Ultimate analysis	
% Carbon	83.38
% Hydrogen	1.82
% Nitrogen	1.47
% Sulfur	0.32
% Oxygen	13.01
H/C	0.26
O/C	0.12
Proximate analysis	
% Moisture	16.62
% Volatile matter	19.76
% Ash	60.68
% Fixed carbon	2.94
pH (1:5 w/v)	10.22
EC (dS m <sup>-1</sup> )	2.60
N <sub>2</sub> adsorption isotherm	
BET surface area (m <sup>2</sup> g <sup>-1</sup> )	69.7
Total pore volume (cm <sup>3</sup> g <sup>-1</sup> )	0.11
BJH most probable pore size (nm)	3.11

Moisture content, however, is much higher than most laboratory-made products. This is likely due to the use of water in the industrial cooling process of biochar production. Particle size distribution of the biochar is not uniform (as shown in Fig. 3), consisting of 38 % of <0.25 mm fraction, 38 % of 0.25–1 mm fraction, and 24 % of 1–3 mm fraction, respectively.

The biochar had a BET surface area of ca.  $80 \text{ m}^2 \text{ g}^{-1}$ . This value was noted to be smaller than reported values for biochars made from similar feedstock and pyrolysis conditions. Strong positive correlations between the BET specific area and pyrolytic temperature have been observed in many previous studies (Mukherjee et al 2001). For instance, the BET values may increase drastically from the range of several to tens of square meters per gram for wood and grass biochars prepared at below  $500 \text{ }^\circ\text{C}$  to several hundred when the temperature increased above  $600 \text{ }^\circ\text{C}$ . This suggests that  $400\text{--}600 \text{ }^\circ\text{C}$  is a transitional range of thermal stability wherein feedstocks go through rapid weight loss and carbonization, resulting in a high surface area (Ahmad et al. 2014). The high ash content may have reduced the BET value of the biochar

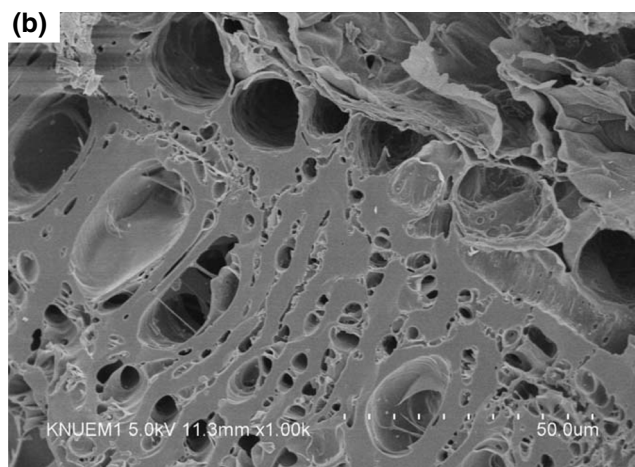
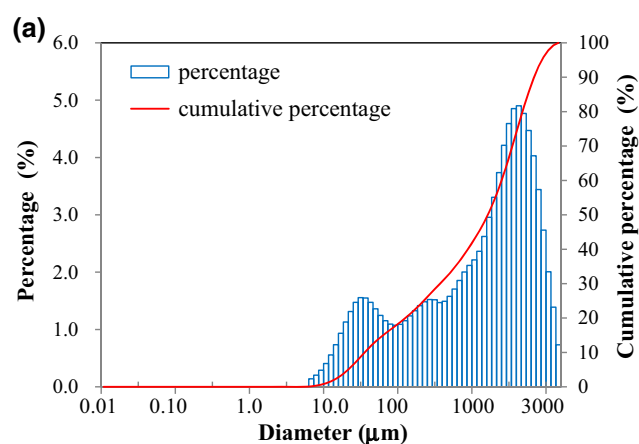


**Fig. 3** **a** Particle size distribution and **b** SEM image (bar  $50 \mu\text{m}$ ;  $\times 1000$  magnification) of the commercial biochar used in this study

used in this study by hindering the formation of microporous structure. However, the biochar might be cost-effective in sorbing certain organic micro-pollutants in soil due to its high aromaticity (Kookana 2010).

### Characterization of biochar pore system using a combination of different methods

Nitrogen adsorption is perhaps the most commonly used approach to determine pores with equivalent radius  $<100 \text{ nm}$  (Greig and Sing 1982). According to definition of the International Union of Pure and Applied Chemistry (IUPAC), the results of the  $\text{N}_2$  adsorption-desorption isotherms (not shown) indicate that the biochar is dominated by mesopores ( $2 \text{ nm} < d < 50 \text{ nm}$ ). Also, the type of the hysteresis loop and the calculated pore size distribution (PSD) show that pores within the biochar particles are mainly in slit shape with size in the range of  $3\text{--}6 \text{ nm}$ .

Suffice it to say, though, that the use of  $\text{N}_2$  adsorption isotherm merely is not adequate for the characterization of biochar inner pore system. As can be clearly observed using SEM scan (Fig. 3), there are abundant channels and pores with radius much larger than  $100 \text{ nm}$ . These pores, particularly of several tens of micrometers in radius, may be a key factor in influencing water retention and permeability of a soil amended with biochar.

In this regard, the present study utilized two liquid media, mercury and water, to examine details of biochar pore organization. Mercury porosimetry uses the non-wetting properties of mercury to gain information on the porous characteristics of solid materials and is extremely suitable for those showing a broad distribution of pore sizes or abundant macropores (Lee et al. 2013; Zhang and You 2013), while water retention is mostly used to predict the soil water storage, water supply to the plants (field capacity) and soil aggregate stability (van Genuchten 1980). This is the first time the conventional water retention method for soil was used to characterize biochar alone.

Corresponding PSDs obtained from the three methods are presented as the logarithmic differentiation  $dv/d\log d$  plotted against a logarithmically spaced pore diameter ( $d$ ) (Supplementary Material, SM2). Three distinct pore size ranges,  $<0.1 \mu\text{m}$ ,  $0.1\text{--}10 \mu\text{m}$  and  $10\text{--}100 \mu\text{m}$ , were identified by mercury porosimetry. The range of  $0.1 < d < 10 \mu\text{m}$  was found to be the most prominent and in a normal distribution, which corresponds to the pores that could retain plant-available water (field water capacity that can be defined as water retained in pores under pressure heads between  $-340 \text{ cm}$  and  $-15,300 \text{ cm}$ ). It is likely that the pores with the size  $<2 \mu\text{m}$  could be formed on the surface of cell wall structures of the feedstock, while the larger pores up to  $100 \mu\text{m}$  may have originated via pyrolysis treatment from the vascular structure of the feedstock. The observation of a small distribution in the range

of  $<0.01 \mu\text{m}$  was consistent with the results of  $\text{N}_2$  adsorption but not well resolved in the porosimeter. This finding was also in agreement with the relatively small microscopic surface area of the biochar, as discussed previously. The third size range of larger pores over  $10 \mu\text{m}$  did not show a normal distribution, which could be attributed to the heterogeneity of the packing voids between the biochar particles rather than inner pores or cavities.

Water retention data obtained by the combination of sand box and pressure plate methods are presented over the whole moisture range from saturation to dryness. Different from infusing gas or mercury into the sample channels under pressure, this approach first saturated the biochar with water and then dehydrated under a series of defined pressures that caused water to flow out of the sample until hydraulic equilibrium was reached (Dane et al. 2002). Significantly, this approach emulates water release (e.g., to plants) rather than water loading during wetting. It is also worth mentioning is that pore size classification in soil science is different from that used in material science. For instance, pores with diameter between 2 and 50 nm are defined as mesopores by colloid and surface chemists. In contrast, according to the Soil Science Society of America (SSSA) (2008), pores are divided into cryptopores ( $<0.1 \mu\text{m}$ ), ultra-micropores (0.1–5  $\mu\text{m}$ ), micropores (5–30  $\mu\text{m}$ ), mesopores (30–75  $\mu\text{m}$ ), and macropores ( $>75 \mu\text{m}$ ). As shown in Supplementary Material, SM2, there are two major distributions with peaks at 0.5 and 100  $\mu\text{m}$ , respectively. The peak corresponding to pores of approximately 1  $\mu\text{m}$  was in agreement with the second distribution observed by the mercury porosimetry but of much lower magnitude. The other larger peak with size above 100  $\mu\text{m}$  was in the range of macropores according to SSSA, which was also consistent with findings by porosimetry but of greater magnitude and shifted towards larger diameters. Similarly, observations of macropores with diameters larger than 10  $\mu\text{m}$  in various biochars have also been reported in previous studies (Brodowski et al. 2005; Zhang and You 2013; Lu et al. 2014).

Figure 4 presents the combined results of PSD curves as determined by the three analytical methods. As for the overlapping pore size ranges characterized by different methods, the method that obtained data with larger magnitude was used. Our results support using the combined methods to gain a detailed PSD over a wide range of equivalent pore size from 0.001 to 1000  $\mu\text{m}$ . The apparent multi-modal PSD indicates the existence of a heterogeneous pore system of the tested biochar. That includes (according to SSSA): cryptopores in the size range of 0.002–0.01  $\mu\text{m}$  that are significant for the adsorption and fate of nutrients and small molecule chemical compounds; micropores with diameter in the range of 0.1–10  $\mu\text{m}$  that can hold plant-available water, and meso- and

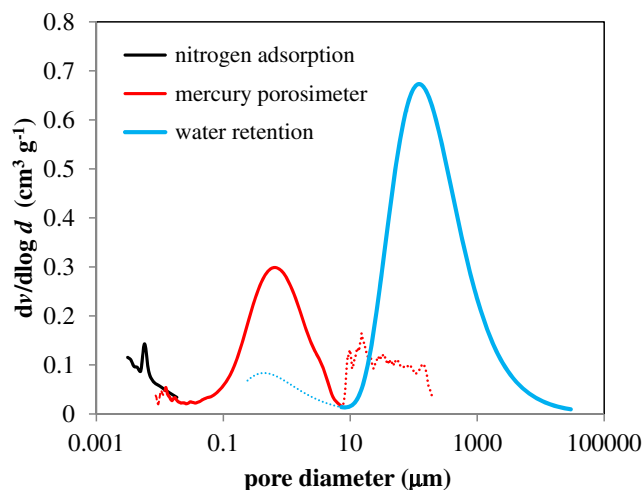


**Fig. 4** Pore size distribution (PSD) of the experimental biochar as determined by the combination of  $\text{N}_2$  adsorption, mercury intrusion and water retention method

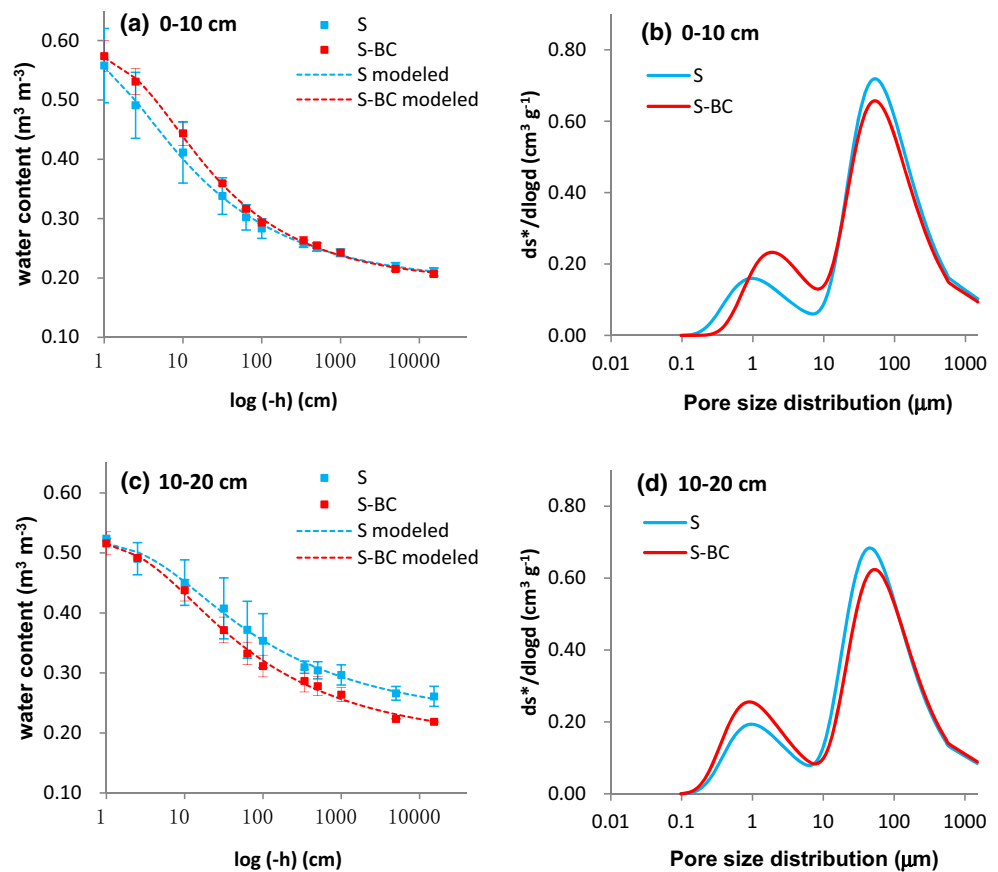
macropores that are particle-packing related. These information together may be useful in explaining the potential effects of biochar amendment on soil properties, particularly the soil PSD and resulting water holding capacity.

#### Effects of biochar application on soil water holding capacity

Figure 5 shows the measured soil water content  $\theta(h)$  and fitted curves (SWRCs) using van Genuchten (1980) soil water retention model and corresponding pore size distributions for the soil cores taken at two depths (0–10 and 10–20 cm) in the plough layer of field plots with and without biochar treatment, respectively. Good fit between the predicted and observed water contents was achieved for both depths of soil with two treatments. It was observed that the SWRCs of the biochar-treated plots were significantly different from those of the controls ( $p < 0.05$ ,  $n = 11$ ).

The corresponding soil physical properties and quality index derived from the fitted SWRC are listed in Table 2. There was a slight decrease in bulk density and increase in total porosity due to the addition of relatively low density biochar particles to the soil. The increased  $S_{\text{inf}}$  index derived at the inflection point of the van Genuchten SWRC for the biochar-treated soil demonstrated improved soil physical qualities as compared to the control treatment. The calculated plant-available water capacity (PAWC) increased from the range of 0.047–0.049 to 0.056–0.068  $\text{m}^3 \text{m}^{-3}$  upon biochar amendment, demonstrating an increase (though not significant) in the soil's capability to hold plant-available water and thus enhance its resistance to drought. Our results are consistent with those of some previous studies that have indicated soil water holding capacity to be significantly increased when

**Fig. 5** Fitted water retention curves to measured data (average  $\pm$ SD, square symbol) using van Genuchten (1980) model and corresponding pore size distributions of soil cores taken at depths of **a–b** 0–10 cm and **c–d** 10–20 cm in the plough layer of field plots with (S-BC) and without (S) biochar amendment. For all regressions,  $R^2 > 0.98$ ,  $n = 11$ ,  $p < 0.01$  (two-tailed)



biomass char material was added (Dugan et al. 2010; Karhu et al. 2011).

As shown in Fig. 5b, d, the experimental soil exhibits a bimodal PSD, with two major peaks occurring at equivalent pore diameter of ca. 1.0 and 50  $\mu\text{m}$ , which are in correspondence to the textural and structural pores, respectively. For both treatments, the dominance of pores with diameters  $>10 \mu\text{m}$  could lead to quick water draining out of the soil upon rainfall events through such PSD and particularly macropores as gravity flow.

Application of the biochar did not change the overall bimodal distribution feature of the soil; however, considerable differences were observed between the control and the biochar treatment. The pore distribution shifted toward smaller pore size range, as reflected by observed greater content of smaller pores (0.1–10  $\mu\text{m}$ ) and lower content of larger pores (10–1,000  $\mu\text{m}$ ), despite that the total porosity of the soil was not significantly changed. Such changing trend was consistent for both soil depths. The raised proportion of textural pores may increase the volume of water influenced by surface forces causing constrained mass flow and thus decrease rapid movement of water under ponded conditions.

The soil pore structure and water holding capacity can be affected by biochar amendment in two ways. Firstly, biochar

itself can hold water in its inner pores and thereby increase the soil water content directly. The potential of such improvement can be determined by the PSD of the packed core of experimental biochar. Our results in this study confirmed the presence of pores with diameters between 0.1 and 10  $\mu\text{m}$  in the biochar that can retain plant-available water. Additionally, other factors such as the total pore volume and hydrophilic functional groups on biochar surface may have also contributed to the enhanced soil WHC, though these effects could be somewhat limited in consideration of the very small amount of biochar added to soil. In contrast to direct influence of biochar on soil water, it can also afford indirect outcomes through its interaction with the soil. Such indirect influences may have been developed over the 1 year of ageing process that was allowed between biochar incorporation and data collection. Such “interaction-effects” have been proposed to be more complex than the binary mixing of two different porous media (Peake et al. 2014). Jien and Wang (2013) argued that the redistribution of the proportion of soil aggregate sizes to be a critical factor in influencing the physical properties of the soil. The incorporated biochar particles could function as a binding agent that connects soil microaggregates to form larger ones and increases pore connectivity and thus improves the soil structure, which in turn increases the soil’s water holding capability.



**Table 2** Comparison of soil properties and van Genuchten hydraulic parameters between the control (S) and biochar-amended soil (S-BC) at two depths in the plough layer of field plots

	0–10 cm		10–20 cm	
	S	S-BC	S	S-BC
Clay (%)	21.2±0.72	18.4±0.32 <sub>a</sub>	19.5±0.40	20.9±3.26
Silt (%)	51.7±4.09	44.4±2.29 <sub>a</sub>	59.0±5.82	52.8±8.16
Sand (%)	27.1±4.16	37.3±2.38 <sub>a</sub>	21.6±6.18	26.2±5.05
Soil organic matter (g kg <sup>-1</sup> )	12.4±0.55	16.9±1.56 <sub>a</sub>	9.8±1.84	12.3±1.54
Bulk density (g cm <sup>-3</sup> )	1.2±0.13	1.1±0.04	1.4±0.08	1.4±0.15
Porosity (m <sup>3</sup> m <sup>-3</sup> )	0.56±0.05	0.58±0.01	0.46±0.03	0.48±0.06
$\alpha$	0.75±0.59	0.31±0.06	0.22±0.58	0.26±0.12
$n$	1.3±0.11	1.4±0.04	1.3±0.18	1.3±0.08
$m$	0.25±0.05	0.28±0.02	0.21±0.10	0.22±0.05
$S_{inf}$	0.07±0.008	0.08±0.009	0.05±0.013	0.06±0.014
$\theta_r$ (m <sup>3</sup> m <sup>-3</sup> )	0.19±0.02	0.19±0.00	0.22±0.07	0.19±0.06
$\theta_s$ (m <sup>3</sup> m <sup>-3</sup> )	0.61±0.05	0.59±0.02	0.52±0.06	0.53±0.03
$\theta_{FC}$ (m <sup>3</sup> m <sup>-3</sup> )	0.26±0.04	0.26±0.05	0.31±0.01	0.29±0.02
$\theta_{PWP}$ (m <sup>3</sup> m <sup>-3</sup> )	0.21±0.05	0.21±0.07	0.26±0.03	0.22±0.02
$\theta_m$ (m <sup>3</sup> m <sup>-3</sup> )	0.32±0.02	0.35±0.03	0.38±0.02	0.35±0.03
MacPor (m <sup>3</sup> m <sup>-3</sup> )	0.29±0.04	0.24±0.05	0.14±0.04	0.17±0.07
AC (m <sup>3</sup> m <sup>-3</sup> )	0.35±0.01	0.33±0.02	0.21±0.03	0.25±0.02
PAWC (m <sup>3</sup> m <sup>-3</sup> )	0.047±0.008	0.056±0.004	0.049±0.010	0.068±0.009

Values are average±S.D. Lower case letters indicate significant differences ( $p < 0.05$ ) between control and biochar treatment at a given depth ( $\alpha$ ,  $n$ , and  $m$  are parameters obtained by fitting the van Genuchten equation to the measured retention data

$\theta_r$  residual water content,  $\theta_s$  saturated water content,  $\theta_{FC}$  water content at field capacity,  $\theta_{PWP}$  water content at permanent wilting point,  $\theta_m$  matrix porosity, *MacPor* macroporosity, *AC* air capacity, *PAWC* plant available water capacity

**Effects of biochar application on DOC transport and quality**

*DOC concentrations of soil pore water and leachate*

Figure 6 shows the concentrations of dissolved organic carbon (DOC) in soil pore waters collected in the plough layer of both the control and biochar-treated field plots upon four rainfall events. Through all rainfalls, the application of biochar to soil significantly increased ( $p < 0.05$ ) the amount of water soluble organic carbon in the layer where biochar was incorporated (at 10 cm) as compared to the control. For the undisturbed subsoil (at 40 cm), DOC concentration was also increased but to a relatively less extent than the top soil, which could be attributed to the vertical transport of DOC. Consistently, the amount of water-extractable organic carbon (WEOC) of the soil was observed to be higher in the biochar treatment (0.0195 mg g<sup>-1</sup>) as compared to the control (0.0157 mg g<sup>-1</sup>). As many previous studies have indicated that biochar addition can increase the soil organic matter (SOM), which is partially contributed from the labile fraction of the biochar carbon (Karhu et al. 2011), we obtained similar results that the SOM in the plough layer was increased by 2.6–4.5 g kg<sup>-1</sup> due to biochar amendment (Table 2). This study also confirmed consistent effects of

biochar amendment on soil organic carbon by the measurements of SOM, WEOC of soil, and DOC of soil pore water at the same time.

As for the leachate, flow samples were obtained only in two of the total five rainfall events, and no surface runoff occurred upon all rainfall events. The results show that DOC

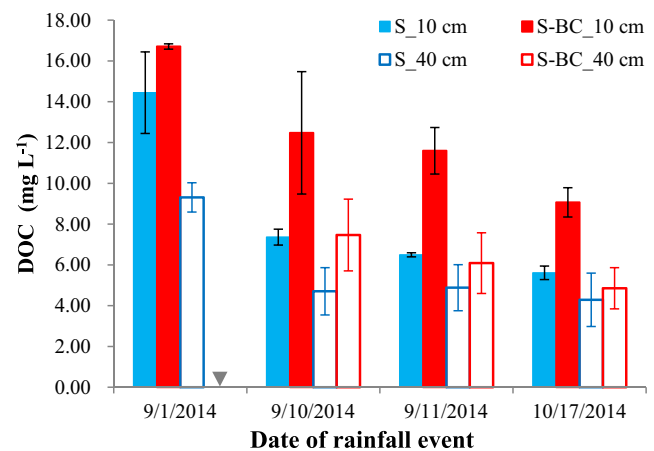


**Fig. 6** Concentrations (average±S.D.) of dissolved organic carbon (DOC) in soil pore water collected upon rainfall events at depths of 10 and 40 cm in the control (S) and biochar-amended (S-BC) field plots (grey inverted triangle: lack of sample)

flux significantly increased from 272 to 346 mg m<sup>-2</sup> after biochar addition to soil ( $p < 0.05$ ). Thus, it is clear that biochar amendment could enhance the formation and loss of DOC from the farmland field, even after 1 year of ageing.

#### Compositional changes in DOC

In addition to the examination of changes in DOC concentrations, fluorescence excitation-emission matrix (EEM) spectroscopy of both soil pore water and leachate samples was analyzed to identify the compositional changes in DOC. Examples of the obtained EEM spectra were shown in the Supplementary Material, SM3. The range of wavelengths for each EEM is limited by an upper Rayleigh-scattering boundary that occurs when the excitation and emission wavelengths are equal and also a secondary-order scattering boundary that occurs at emission wavelengths that are approximately twice the values of the excitation wavelengths (both scatterings have been removed via data processing). Based on the fluorescence regional integration technique, EEM was divided into three regions, as outlined on one spectrum in SM3, with their corresponding  $\lambda_{ex}/\lambda_{em}$  ranges on the EEM contour map being 250–300/310–390 nm (region I), 250–300/390–520 nm (region II), and 300–420/310–520 nm (region III), respectively. Operationally, DOC fluorophores in these regions are assigned to protein-like species or soluble microbial products (SMPs), fulvic-like, and humic-like species, respectively (Henderson et al 2009).

By visual observation, biochar treatment resulted in higher intensities in all EEM regions as compared to the control. However, due to the fact that values of DOC vary between samples and that the fluorescence intensity is generally correlated positively with DOC concentration, direct comparison of original EEM spectra between the samples gives very limited information. In this light, the total intensity for each DOC component was calculated with the intensity normalized by DOC concentration of each sample.

The obtained results are shown in Fig. 7. Generally, the proportion of the three distinct groups of fluorophores follows the order of fulvic-like > humic-like > protein-like species for both soil pore water and leachate samples and also for both treatments, being consistently associated with their soil-related qualities. The contribution of the protein-like species to the sample DOC should be very small in consideration that this group of fluorophores usually has a quite high fluorescence efficiency. The soil pore water collected in the plough layer (10 cm) has a relatively greater fluorophore content per unit of DOC than that in the subsoil layer (40 cm), which is probably due to the abundance of crop debris and plant residues in the surface soil that could yield highly water soluble organic carbon such as protein, cellulose and polysaccharide (Boyer and Groffman 1996; Stevenson and Cole 1996). The leachate has the lowest content of fluorophores.

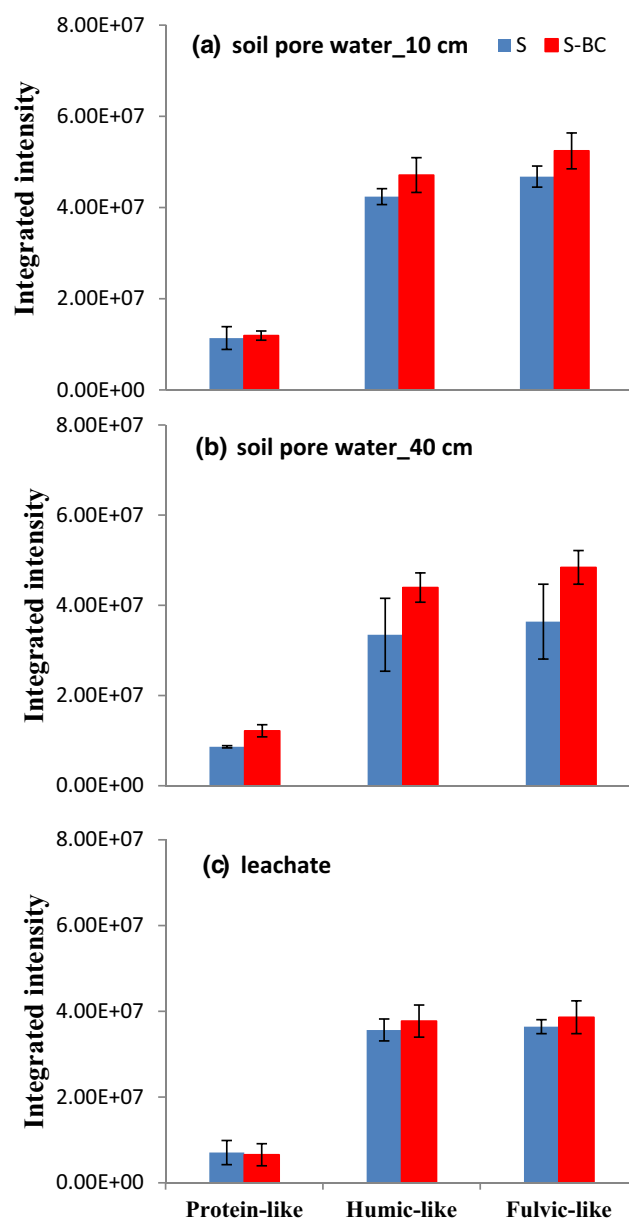


**Fig. 7** EEM fluorescence intensity (average  $\pm$  SD) of different chromophoric components of dissolved organic carbon (DOC) for **a–b** soil pore water and **c** leachate collected upon a rainfall event (Sept. 11, 2014) in the control (S) and biochar-amended (S-BC) field plots

As compared to the control, biochar amendment led to an increased content of fluorophores of all groups in the DOC matrix. This observation was also consistent with no exception for all investigated rainfall events. In spite of the increased amount of fluorophore species, on the other hand, none of the proportional distribution of the fluorophores, the index of aromaticity ( $SUVA_{254}$ ), and humification had been significantly changed ( $p > 0.05$ ; data not shown). Thus, we assume that the DOC increment in biochar-amended plots came primarily from the soil organic carbon pool rather than the direct contribution from the biochar itself. This makes sense due to the fact that the weight percentage the biochar added to soil is very small on the one

hand, and the biochar-derived DOC is different from the soil-originated components whose differences can be identified in the EEM on the other hand (Jamieson et al. 2014). We also argue that the effects of biochar application lie in the interactions between biochar and SOM which involve complicated microbial and fermentation processes that together will determine the production and speciation of DOC (Aguilar and Thibodeaux 2005). Also, the process of DOC formation is strongly influenced by the factors including temperature, soil water content, and in particular wet-dry cycles (Chow et al. 2006). Future work is needed to fully understand the biochar's role in these processes under varying field moisture conditions on the basis of examination of relevant mechanisms.

### Conclusions

To sum up, application of a commercial biochar increased the plant-available water capacity (PAWC) of the studied soil. The use of a combination of three pore size distribution characterization methods, N<sub>2</sub> adsorption, mercury intrusion, and water retention, showed that the biochar has a heterogeneous pore system showing tri-modal distribution. It should be noted the pores in the size range of 0.002–0.01 μm that are significant for the fate of nutrients and small molecule contaminants, while the pores with diameter between 0.1 and 10 μm are important for retaining water available to plants. Biochar amendment increased PAWC in the experimental soil from the range of 0.047–0.049 to 0.056–0.068 cm<sup>3</sup> cm<sup>-3</sup>. However, accelerated leaching of carbon in the form of dissolved organic carbon (DOC) upon rainfall events was observed even a year after biochar application. Biochar treatment also increased soil organic matter content, water-extractable organic carbon in the soil and DOC concentration in soil pore water and leachate. Future work is needed to continuously monitor and evaluate the long-term effects of biochar application on the farmland soil properties and carbon cycling and transformation at interfaces between air-soil-groundwater.

**Acknowledgments** Support for this work is provided by Nature Science Foundation of China (41301549, 21307152, and 41471268), China Postdoctoral Science Foundation (2013M530408), and CAS-SAFE International Partnership Project (KZZD-EW-TZ-06). Thanks also goes to the Hundred Talents Program of CAS for supporting activities related to the data processing and preparation of this manuscript.

### References

Aguilar L, Thibodeaux LJ (2005) Kinetics of peat soil dissolved organic carbon release from bed sediment to water. Part 1. Laboratory simulation. *Chemosphere* 58:1309–1318

Ahmad M, Rajapaksha AU, Lim JE et al (2014) Biochar as a sorbent for contaminant management in soil and water: a review. *Chemosphere* 99:19–33

Asai H, Samson BK, Stephan HM et al (2009) Biochar amendment techniques for upland rice production in Northern Laos 1. Soil physical properties, leaf SPAD and grain yield. *Field Crop Res* 111:81–84

Atkinson CJ, Fitzgerald JD, Hipps NA (2010) Potential mechanisms for achieving agricultural benefits from biochar application to temperate soils: a review. *Plant Soil* 337:1–18

Boyer JN, Groffman PM (1996) Bioavailability of water extractable organic carbon fractions in forest and agricultural soil profiles. *Soil Biol Biochem* 28:783–790

Brodowski S, Amelung W, Haumaier L et al (2005) Morphological and chemical properties of black carbon in physical soil fractions as revealed by scanning electron microscopy and energy-dispersive X-ray spectroscopy. *Geoderma* 128:116–129

Case SDC, McNamara NP, Reay DS et al (2013) Can biochar reduce soil greenhouse gas emissions from a *Miscanthus* bioenergy crop? *GCB Bioenergy* 6:76–89

Chen W, Westerhoff P, Leenheer JA et al (2003) Fluorescence excitation-emission matrix regional integration to quantify spectra for dissolved organic matter. *Environ Sci Technol* 37:5701–5710

Chow AT, Tanji KK, Gao S et al (2006) Temperature, water content and wet-dry cycle effects on DOC production and carbon mineralization in agricultural peat soils. *Soil Biol Biochem* 38:477–488

Cornelis WM, Khlosi M, Hartmann R et al (2005) Comparison of unimodal analytical expressions for the soil-water retention curve. *Soil Sci Soc Am J* 69:1902–1911

Dane JH, Hopmans JW, Romano N et al (2002) Soil water retention and storage-laboratory methods. In: Dane JH, Topp GC (eds) *Methods of soil analysis part 4-physical methods*. Soil Science Society of America, Madison, pp 675–720

Dexter AR (2004) Soil physical quality. Part I: theory, effects of soil texture, density, and organic matter, and effects on root growth. *Geoderma* 120:201–214

Dugan E, Verhoef A, Robinson S et al (2010) Bio-char from sawdust, maize stover and charcoal: Impact on water holding capacities (WHC) of three soils from Ghana. *Proceedings of the 19th World Congress of Soil Science, Soil solutions for a changing world*, Brisbane, Queensland, Australia, 8:1–6

Gerrity D, Gamage S, Jones D et al (2012) Development of surrogate correlation models to predict trace organic contaminant oxidation and microbial inactivation during ozonation. *Water Res* 46:6257–6272

Gregg SJ, Sing KSW (1982) *Adsorption, surface area, and porosity*. Academic Press, London

Guggenberger G, Rodionov A, Shibistova O et al (2008) Storage and mobility of black carbon in permafrost soils of the forest tundra ecotone in Northern Siberia. *Glob Chang Biol* 14:1367–1381

Henderson RK, Baker A, Murphy KR et al (2009) Fluorescence as a potential monitoring tool for recycled water systems: a review. *Water Res* 43:863–881

Hernandez-Ruiz S, Abrell L, Wickramasekara S et al (2012) Quantifying PPCP interaction with dissolved organic matter in aqueous solution: combined use of fluorescence quenching and tandem mass spectrometry. *Water Res* 46:943–954

Hockaday WC, Grannas AM, Kim S et al (2007) The transformation and mobility of charcoal in a fire-impacted watershed. *Geochem Cosmochim Acta* 71:3432–3445

Jamieson T, Sager E, Guéguen C (2014) Characterization of biochar-derived dissolved organic matter using UV-visible adsorption and excitation-emission fluorescence spectroscopies. *Chemosphere* 103:197–204

Jeffery S, Verheijen FGA, van der Velde M et al (2011) A quantitative review of the effects of biochar application to soils on crop productivity using meta-analysis. *Agric Ecosyst Environ* 144:175–187

Jien SH, Wang CS (2013) Effects of biochar on soil properties and erosion potential in a highly weathered soil. *Catena* 110:225–233

- Karhu K, Mattila T, Bergström I et al (2011) Biochar addition to agricultural soil increased CH<sub>4</sub> uptake and water holding capacity—results from a short-term pilot field study. *Agric Ecosyst Environ* 140:309–313
- Kookana RS (2010) The role of biochar in modifying the environmental fate, bioavailability, and efficacy of pesticides in soils: a review. *Aust J Soil Res* 48:627–637
- Korshin GV, Wu WW, Benjamin MM et al (2002) Correlations between differential absorbance and the formation of individual DBPs. *Water Res* 36:3273–3282
- Laird DA, Fleming P, Davis DD et al (2010) Impact of biochar amendments on the quality of a typical Midwestern agricultural soil. *Geoderma* 158:443–449
- Lee Y, Park J, Ryu C et al (2013) Comparison of biochar properties from biomass residues produced by slow pyrolysis at 500 °C. *Bioresour Technol* 148:196–201
- Lehmann J, Gaunt J, Rondon M (2006) Biochar sequestration in terrestrial ecosystems—a review. *Mitig Adapt Strat Glob Chang* 11:403–427
- Lu SG, Sun FF, Zong YT (2014) Effect of rice husk biochar and coal fly ash on some physical properties of expansive clayey soil (Vertisol). *Catena* 114:37–44
- Mukherjee A, Zimmerman AR (2013) Organic carbon and nutrient release from a range of laboratory-produced biochars and biochar-soil mixtures. *Geoderma* 193–194:122–130
- Mukherjee A, Zimmerman AR, Harris W (2001) Surface chemistry variations among a series of laboratory-produced biochars. *Geoderma* 163:247–255
- Nelissen V, Ruyschaert G, Manka'Abusi D et al (2015) Impact of a woody biochar on properties of a sandy loam soil and spring barley during a two-year field experiment. *Eur J Agron* 62:65–78
- Peake LR, Tang X, Reid BJ (2014) Quantifying the influence of biochar on the physical and hydrological properties of dissimilar soils. *Geoderma* 235–236:182–190
- Reynolds WD, Drury CF, Yang XM et al (2007) Land management effects on the near-surface physical quality of a clay loam soil. *Soil Tillage Res* 96:316–330
- Soil Science Glossary Terms Committee (2008) Glossary of Soil Science Terms 2008. Soil Science Society of America, Madison
- Stevenson FJ, Cole MA (1996) Cycles of soil: carbon, nitrogen, phosphorus, sulfur, micronutrients (second ed.). Wiley, New York
- Tammeorg P, Simojoki A, Mäkelä P et al (2014) Biochar application to a fertile sandy clay loam in boreal conditions: effects on soil properties and yield formation of wheat, turnip rape and faba bean. *Plant Soil* 374:89–107
- van Genuchten MT (1980) A closed form equation for predicting the hydraulic conductivity of unsaturated soils. *Soil Sci Soc Am J* 44:892–898
- Veksha A, McLaughlin H, Layzell DB et al (2014) Pyrolysis of wood to biochar: increasing yield while maintaining microporosity. *Bioresour Technol* 153:173–179
- Vomocil J, Flocker W (1965) Degradation of structure of Yolo loam by compaction. *Soil Sci Soc Am J* 29:7–12
- Washburn EW (1921) The dynamics of capillarity flow. *Phys Rev* 17:273–283
- Zhang J, You CF (2013) Water holding capacity and absorption properties of wood chars. *Energy Fuel* 27:2643–2648